Distribution Agreement

In presenting this thesis as a partial fulfillment of the requirements for a degree from Emory University, I hereby grant to Emory University and its agents the non-exclusive license to archive, make accessible, and display my thesis in whole or in part in all forms of media, now or hereafter now, including display on the World Wide Web. I understand that I may select some access restrictions as part of the online submission of this thesis. I retain all ownership rights to the copyright of the thesis. I also retain the right to use in future works (such as articles or books) all or part of this thesis.

Nwamaka Ijeh April 4, 2021

Pathological Characterization of AAV2-Flex-taCaspa3-2A-TEVp-Induced Temporal Lobe Epilepsy in a Mouse Model

by

Nwamaka Ijeh

Claire-Anne Gutekunst, PhD

Adviser

Neuroscience and Behavioral Biology

Claire-Anne Gutekunst, PhD

Adviser

Michael Crutcher, PhD

Committee Member

Saadein Reza, PhD

Committee Member

2021

Pathological Characterization of AAV2-Flex-taCaspa3-2A-TEVp-Induced Temporal Lobe Epilepsy in a Mice Model

By

Nwamaka Ijeh

Claire-Anne Gutekunst, PhD

Adviser

An abstract of
a thesis submitted to the Faculty of Emory College of Arts and Sciences
of Emory University in partial fulfillment
of the requirements of the degree of
Bachelor of Science with Honors

Neuroscience and Behavioral Biology

2021

Abstract

Pathological Characterization of AAV2-Flex-taCaspa3-2A-TEVp-Induced Temporal Lobe Epilepsy in a Mice Model

By Nwamaka Ijeh

Temporal lobe epilepsy (TLE) affects 6 out of 10 people with focal epilepsy. It is characterized by (i) severe hippocampal atrophy, (ii) limited extra hippocampal damage, (iii) latent period between beginning of spontaneous recurrent seizures and progressive epilepsy (iv) neuronal loss in the subiculum-CA1, CA3 and the dentate hilus, (v) localization of seizure foci in the amygdala. Mice models of epilepsy are used to better elucidate mechanisms of TLE and test treatment options. Most mice models using chemo convulsants, like Kainic acid or Pilocarpine, to create spontaneous recurrent seizures and mimic some of the damaged characteristics observed in human TLE. However, they provide results with lots of variability in neuropathology, and extensive damage to the hippocampus, and loss of subjects - up to 30% mortality. Since depletion of GABAergic neurons creates an imbalance of excitation and inhibition which increases occurrence of spontaneous recurrent seizures, this study aims to induce apoptosis of GABAergic neurons using AAV2-Flex-taCaspa3-2A-TEVp to model pathology of TLE. Injecting the dorsal and ventral hippocampi with rAAV2-Flex-taCaspa3-2A-TEVp at a rate of 200 nl/min caused significant loss of neurons in dentate gyrus hilus, CA1 and CA3 Stratum Oriens (SO) and Stratum Radiatum (SR) regions. Also, loss of GABAergic neurons in these regions of the hippocampus was also observed. The greatest loss of neurons was found closest to the site of injection, and a loss of volume was observed in the injected hemisphere. Furthermore, reactive gliosis was observed in the injected side of the brain. This model of TLE caused SRSs and had the key characteristics of TLE typically observed in human tissue.

Pathological Characterization of AAV2-Flex-taCaspa3-2A-TEVp-Induced Temporal Lobe Epilepsy in a Mice Model

By

Nwamaka Ijeh

Claire-Anne Gutekunst, PhD

Adviser

A thesis submitted to the Faculty of Emory College of Arts and Sciences
of Emory University in partial fulfillment
of the requirements of the degree of
Bachelor of Science with Honors

Neuroscience and Behavioral Biology

2021

Acknowledgements

My thanks to Claire-Anne Gutekunst, my advisor, whose constant support, and encouragement helped me grow throughout the past two years. I am grateful for the time and effort she put into explaining the various aspects of the projects: viral vector, and methods of analysis, to me. I would also love to thank Alejandra Fernandez, PhD for helping me with the statistical analysis and listening to my ideas when trying to understand concepts in the lab. I would also love to thank my committee members for their support and feedback throughout the process. I would also love to thank my parents for their unrelenting support throughout the past four years.

Table of Contents

Introduction

Epilepsy is the most common neurologic disorder as it affects about 1% of the world's population (Ngugi et al., 2010). Approximately 3.2 – 3.4 million people in the United States live with epilepsy (Zack and Kobau, 2017), of those people about 25% percent suffer from temporal lobe epilepsy (TLE). TLE is the most common form of focal seizures originating from the electrical abnormality of the temporal lobe (Zhao et al., 2014). TLE is characterized by pronounced hippocampal atrophy and limited extrahippocampal damage (Kienzler-Norwood et al., 2017), a latent period and unilateral hippocampal lesion characterized by neuronal loss in the subiculum-CA1 and the dentate hilus, localization of seizure foci in the amygdala, entorhinal cortex (Levesque and Avoli, 2013). TLE not only causes spontaneous recurrent seizures (SRSs) that can be observed clinically, but they also create impairments in aspects of cognitive functioning including executive function, memory, and language impairments (Chin and Scharfman, 2013). Causes of TLE are unknown, however, brain insults, head trauma or prolonged febrile seizures could set the stage for progression of TLE (Jensen et al., 2000).

To better understand the disorder's ontogenesis and develop better therapeutic interventions, animal epilepsy models are utilized. An ideal TLE animal model would fulfill (a) face validity: animal model would reproduce the phenotypes observed with the human disease, (b) constructive validity: exact human cause e.g., mutation or injury that caused the disease, (c) predictive validity: effectiveness of model to predict the outcome of future interventions and recapitulate treatment responsiveness. However, most of the animal models used are isomorphic (Falcon-Moya et al., 2018), meaning it duplicates the human disease without replicating the etiology because TLE has several etiologies. Several animal models of TLE have been developed however, each comes with their drawbacks and fail to present all three model validities as described above.

Animal Model of TLE: Chemo-convulsants

The most common type of animal models used for TLE research induce a disease state via delivery of chemo-convulsants like kainic acid (KA) or pilocarpine directly into the hippocampus or systemically. KA is a L-glutamate analog that can induce neurodegeneration and acute seizures in rodents through the activation of kainate receptors in hippocampal neurons (Berger et al., 1990). Generally, KA mimics bilateral neuronal damage like loss of pyramidal cells in CA1, CA3and dentate gyrus (CA4), neurodegeneration in the caudate putamen and bilateral gliosis which are observed in human TLE (Stafstrom, 2005). Pilocarpine, a muscarinic acetylcholine receptor agonist, provides another model of TLE after systemic/targeted injections that results in a darkened and shrunken pyramidal cell layer within the hippocampus (Furtado et al., 2011). Pilocarpine induces status epilepticus (SE) by causing elevation of glutamate levels in the hippocampus which creates an imbalance between inhibitory and excitatory transmission (Costa et al., 2004).

Both KA and pilocarpine models have unique advantages and disadvantages. Intrahippocampal delivery of KA induces hippocampal sclerosis and SRSs. Also, it produces variable hippocampal injury with most of the damage occurring in the extrahippocampal regions. Systemic KA injection, either intraperitoneal or subcutaneous, requires no surgical procedure and induces SRSs and hippocampal sclerosis without brain damage from cannulation. However, this method provides no regulation over the bioavailability of KA in the brain, the amount of KA differs between subjects (Zheng et al., 2010, Rusina et al., 2021 and Rocha, 2009). Also, if SRSs are achieved, it typically is followed by major neuronal loss in extrahippocampal, extensive bilateral gliosis, brain edema, neuronal loss in the substantia nigra, thalamus and mesencephalon.

It also has a mortality rate of up to 30% as well as 20-40% non-responders (never develop seizures) (Kienzler-Norwood et al., 2017). As for pilocarpine models, once seizures are initiated through M1 receptors, they are sustained by activation of NMDA receptors (Kapur, 2018, Imtiyaz and Juvale, 2020). Systemic administration of pilocarpine promotes an acute period, that later develops into a limbic status epilepticus which usually lasts 24 hours. It is then followed by a latent period that ranges from 4 to 44 days. After this latent period, a chronic period with SRSs and widespread lesions resembling those seen in human TLE and associated neuronal network reorganization in hippocampal and parahippocampal regions (e.g., mossy fiber sprouting and interneuron loss). Mortality rate of pilocarpine models is about 30-40% in rat subjects (Curis et al., 2008). KA and pilocarpine models have been a staple in the field for modeling epilepsy. However, the high mortality rates, inconsistencies between subjects, and variable results in responders requires a reconsideration of these models.

There are other, non-drug induced ways of modeling TLEs, however, they too have their drawbacks. For example, audiogenic models that induce TLE by acoustic stimulation in genetically prone animals manifests wild running and tonic-clonic seizures (Hubbard and Binder, 2016). However, it is unable to produce behavioral SRSs without a trigger. Hypoxia models which bring repetitive and brief tonic-clonic seizures by exposing rodents to air with low O_2 concentrations are also flawed because the vulnerability for seizures varies with the age and strain of the rodents (Kandratavicius et al., 2014). In general, the already established models of TLE are less tunable, provide results with lots of variability in neuropathology, and extensive damage to the hippocampus that sometimes causes loss of subjects - up to 30% mortality (Levesque and Avoli, 2016).These drawbacks of the TLE models above beg for a more reliable and targeted approach.

Observing both KA-based and pilocarpine models, we have observed that they produce significant loss of pyramidal neurons in the CA layers as well as a reduction in and damage of GABAergic interneurons, rather than principal neurons (Fritsch et al., 2009). This suggests that GABAergic neurons in the hilus, CA1 and CA3 are highly vulnerable to recurrent seizures. The loss of GABAergic interneurons disrupts the balance of excitation and inhibition to favor excitation. Further, an elimination of GABAergic receptors due to chemo-convulsant administration disrupts the control of the excitatory network causing the higher possibility of generating SRSs that produce long-lasting epileptiform discharges in KA and pilocarpine treated animals (Knopp et al., 2005). These results suggest that selectively targeting GABAergic neurons may provide improved epileptic animal models.

Therefore, since depletion of GABAergic neurons is known to increase occurrence of SRSs, several studies have specifically targeted GABAergic interneurons with the goal that these models would be more selective and less likely to produce unnecessary widespread damage and high mortality. Recent studies have permanently inhibited GABA release from parvalbumin (PV) interneurons of the ventral subiculum using either AAV2-hSyn-FLEX-hM4Di-mCherry plasmid or SSP-Saporin. Their results showed a continuous spike wave discharge that further developed into the SRSs; however, this model was not chronic as SRS stopped after four days and only mimicked a few of the characteristics of TLE like loss of PV-containing interneurons are in the subiculum and Ammon's horn sclerosi (Drexel et al., 2017; Chun et al., 2019).

Therefore, the aim of this study is to pathologically characterize AAV2-Flex-taCaspa3-2A-TEVp-induced TLE model. The AAV2-Flex-taCaspa3-2A-TEVp employs a genetically engineered caspase-3, whose activation by tobacco etch virus protease (TEVp) commits a Cre+ cells to apoptosis. The generated adeno-associated virus (AAV) is used to carry the DNA into

cells and ensures that the virus targets neurons. Since Vgat-Cre mice expresses Cre recombinase in all vesicular GABA transporter (Vgat) expressing cells, the apoptosis inducing caspase-3 is only activated in GABAergic cells. The T2A peptide encodes sequence to ensure the separation of taCasp3 from TEVp after they have been translated. We will be analyzing the effect of this model to observe if there is a decrease in GABAergic neurons, analyzing the effect of distance from Bregma in the injected sides, observing whether extensive gliosis occurs in the injected side. We expect this model to mimic TLE characteristics when tissues are analyzed during histology: stereology and immunostaining. A loss of neurons in CA1, CA3 and DG, specific loss of GABAergic neurons in CA1 and Hilus should be observed alongside inflammation and volume loss.

Material and Methods

Subjects: Adult (10-12 week-old - 18-25 g) heterozygous Vgat-ires-cre mice bred in our animal facility from homozygous Vgat-ires-cre male mice (Jackson Laboratory, Stock#028862) and C57BL6 wild type females (Jackson Laboratory, Stock#000664) were used. Mice were maintained on a 12 h light cycle (lights off from 7pm-7am) with ad libitum access to food and water. All procedures were conducted in accordance with the Guide for the Care and Use of Laboratory Animals, as adopted by the IAUCU, and with approval of the Institutional Animal Care and Use Committee at the Emory University.

Viral Constructs: Purified and concentrated adeno-associated viruses coding for taCasp3 (AAV2-Flex-taCaspa3-2A-TEVp) were all packaged by the UNC Vector Core Facility at 4x10^12 viral molecules/mL.

Stereotactic surgeries: Adult heterozygous Vgat-ires-cre males were anesthetized with isoflurane (3% for induction, 1.5% for maintenance) and fixed on a stereotaxic apparatus. The dorsal and ventral hippocampi were targeted for injection using the following coordinates: AP:--2.53mm, ML:+/-2.0 mm, and DV:-1.8 mm for dorsal injections; AP:-3.7 or -3mm, ML:+/-2.76 mm, DV:-3.0 mm for ventral injections. Two (n = 6) or three (n = 3) 0.5-µl injections of rAAV2-Flex-taCaspa3-2A-TEVp (4x10^12 viral molecules/mL, UNC GTC Viral Vector Core) were injected through a glass-pulled pipette using a Nanoject injector (Drummond Scientific, Broomall, PA) at a rate of 200 nl/min and allowed to equilibrate for 5 minutes in the brain before and after each injection. After completing the virus injections, mice were implanted with a premade headplate (Zhu, Aiani et al. 2020) containing two hippocampal depth electrodes (AP:-2.53mm; ML:+/-2.0mm; DV:-1.8mm), a frontal (AP:+1.0mm; ML:+1.3), a parietal (AP:-1.5mm; ML:-2.8mm) EEG screw electrode, a reference screw (AP:-6.0mm; ML:0mm), and a ground screw (AP:+1.0mm; ML:-1.3mm), and two EMG leads placed over the neck muscles. Mice were allowed to recover for 4-7 days before starting the recording experiments. Following the surgery, mice were housed individually. Synchronized video-EEG/EMG signals were recorded using a Blackrock Microsystems Cerebus™ Neural Signal Processor using Central software (Microsystems LLC, Salt Lake City, UT) and began the day after virus injection and continued for 40 days. Signals were sampled at 2 kHz without online filtering. Recordings were saved and restarted remotely every 24 h**.**

Immunohistochemistry: At the end of experimentation mice were euthanized with an overdose of sodium pentobarbital (100 mg/kg, ip). Anaesthetized mice were transcardially perfused with

saline followed by 4% paraformaldehyde (PFA) in 0.1 M phosphate buffer. Brains were removed and postfixed in the same fixative by immersion overnight at room temperature at 4°C and then switched to 30% sucrose until they sank. Coronal sections 40 µm thick were cut using a cryostat (Leica) and collected as floating sections in 1x PBS. Sections were then blocked in 4% Normal donkey serum (Jackson ImmunoResearch, Lot: 152717) , 0.1% Triton X-100, and 1 X PBS for 30 minutes at room temperature. Primary antibodies: GFP (1:1000, rabbit polyclonal, Z0334, DAKO), 2% of NDS and NeuN (1:2000, mouse polyclonal, MAB377, MAB377) were diluted in 1 X PBS and incubated on an orbital shaker for >24 h at 4°C temperature. Sections were washed in PBS. Secondary antibodies: 40 ul of NDS, 4ul donkey anti-mouse (1:500, Alexa Fluor 488 donkey, Lot: 1113537, anti-mouse IgG (H+L)), and 2% of donkey anti-rabbit (1:500, Lot: 105217) diluted in 1 X PBS. Sections were washed in PBS and mounted on microscope slides (Fisherbrand; 25 x 75 x 1.0mm) for fluorescence microscopy.

Unbiased Stereology: Stereological estimation of total neurons in several circuits of the hippocampus was performed on both hemispheres of the brain following a similar protocol described by Bird et al., 2018. The brain was extracted from the skull, and each brain was immersed in 10% buffered formalin for a duration of time. The tissue was then placed into a cryoprotectant solution in preparation for freezing. The tissue was sliced into coronal sections (40 µm thick) using a Leica cryostat and stained with the standard Nissl method for further analyses. Stereology was performed using an optical fractionator probe of unbiased stereological cell counting method using the Leica Microsystems**.** Every 40 µm coronal section through the dorsal hippocampus (lateral coordinate number in mm e.g., 0.36 - 2.52mm using to the Paxinos adult mouse brain atlas (Paxinos and Franklin, 2013)) was counted. Damaged selected sections

were replaced using the closet intact section. Similar and uniform contours were manually traced around the dentate gyrus hilus, CA1 and CA3. All regions examined had a dissector height was 5µm, guard height was 2µm, frame area was 25% screen and frame spacing was 100µ**.** The number of neurons of CA1, CA3 and Hilus were estimated using the uniform contours drawn around each hippocampal subregion.

Image Analysis using ImageJ Software: Image acquired by automated microscopy from the Vgat-tom mice was loaded into the ImageJ software program. The images from Vgat-tom mice expressed both tdTomato (red fluorescent reporter) and Cre recombinase in all vesicular GABA transporter expressing cells. Therefore, the tdTomato (red fluorescent) was only in GABAergic cells and observed as bright pixel on the image. The cell counter plug-in was loaded and the desired image for counting was initialized. Counter type one was selected for the left side of the hippocampus while counter type two was selected for the right side of the hippocampus. Each cell was manually counted for the DG and CA1. Manual cell counts were not performed on CA3 because this region had a dense population of cells that overlap each other. Integrated densities were performed on DG, CA1 and CA3 by keeping the area of selected region constant for each section and measuring the intensity of pixels present in selected region**.**

Image analysis using Cell Profiler: Images acquired by automated microscopy from the Vgat-tom mice were loaded into the Cell Profiler program (Broad Institute, Cambridge, MA). The process had four main steps: rescale intensity, enhance and suppress features, identification of primary objects and measurement of object intensity. The first task, performed by CellProfiler, was rescaling the intensity of the images. This CellProfiler module used the full intensity range

by stretching each image. After, finding the minimum and maximum values of the unmasked whole image, every pixel was rescaled so that the minimum intensity was set to zero and the maximum values had an intensity of one. The second task performed by CellProfiler was to enhance or suppress the features of the image which improved the subsequent identification of primary objects. This module suppressed the background and enhanced the intensity of specific pixels by applying image processing filters to the whole image. The product was a greyscale image where objects could easily be identified using the identify module. The next task was to identify primary objects. Identify Primary Objects module identifies biological objects of interest (GABAergic neurons with similar morphology, high intensity contrast when compared to the background and good separation between adjacent cells). The next task was performed by the measure object intensity module which measured intensity features of identified primary objects to ensure that similar objects were counted. From the image created by the identify primary objects module (GABAergic cells), intensity features were extracted for each object based on its corresponding grayscale images. Measurements were recorded for each object. The last module within the pipeline (Export to Database).

Statistical Analysis: Nissl stereology counts were presented as the estimated total number of neurons for both injected and non-injected sides**.** All data for integrated densities are presented as mean ± SEM. Statistical analysis were assessed using paired t tests when data passed Shapiro-Wilk or Kolmogorov-Smirnov normality test. However, a Wilcoxon-rank sum test was performed when data did not pass normality test. Non-significance was defined as $p \geq 0.05$ and significance as $*p < 0.05$. Statistical analyses were performed with GraphPad Prism 5.0 (GraphPad Software, Inc., San Diego, CA).

Results

Qualitative Overview of Nissl-Stained Sections

A representative image of a Nissl-stained section with both injected and non-injected sides is provided (Figure 1). Each desired region of the hippocampus is labelled. The Dentate gyrus (DG)- hilus was defined as the region in between the densely packed- granular cells layers. CA1 Stratum Oriens (SO) was defined as the region above the densely packed pyramidal cells. CA1 SO contains cell bodies of inhibitory basket cells. CA1 Stratum radiatum (SR) was defined as the region below the densely packed- granular cells layers. CA3 SO and SR were defined like CA1 SO and SR, however the CA3 region is found closer to the hilus while the CA1 regions are seen above the DG hilus. These areas in the hippocampus were chosen for stereological analysis because they contain large populations of GABAergic interneurons (Maccaferri, 2005 and Losonczy et al., 2002).

Loss of Neurons in Dentate Gyrus Hilus, CA1 and CA3 Stratum Oriens (SO) and Stratum Radiatum (SR) Regions

To determine whether AAV CAS injection resulted in a loss of neurons, the number of neurons in each hippocampal region was estimated using unbiased stereology (Figure 2). In the dentate gyrus, there was a significant loss of neurons, Figure 2a shows the stereology counts in the dentate gyrus hilus of both injected and non-injected sides. There was an overall significant decrease in the number of neurons in the injected side of the hilus (*$p = 0.0009$, $t= 4.683$, $n = 11$, paired t-test). In the CA1 SO and SR there was also a significant decrease of neurons in the injected side of the brain hemisphere (Figure 2b. CA1 SO *$p = 0.0001$, $t = 11.33$, $n =11$. Figure 2c. CA1 SR *$p = 0.0157$, $t= 2.906$, $n = 11$, paired t-test). Lastly, a significant decrease in neurons

present in the injected sides of both CA3 SO and SR compared to the non-injected sides was found (Figure 2d. CA3 SO *p = 0.0133, t= 3.002, n = 11. Figure 2e. CA3 SR *p = 0.0015, t = 4.330, n =11, paired t-test). The area surrounding the molecular layer down to granule layer of the hilus of the injected side experienced shrinkage (Figure f and g).

Loss of GABAergic Neurons in Dentate Gyrus Hilus, CA1 and CA3 Stratum Oriens (SO) and Stratum Radiatum (SR) Regions

Nissl-stained sections analyzed through stereology provided information about the decrease in total neurons in each specific region. However, because this project aimed to specifically target GABAergic cells, analysis done on Vgat-tom mice images using ImageJ and Cell profiler gave information about changes in GABAergic neurons. The analysis of total number of GABAergic interneurons in subject #12 in both DG-hilus and CA1 is provided in Figure 3. The data sets in these figures did not pass the Shapiro-Wilk test, therefore a one sample Wilcoxon test was performed to examine if there was a significant difference in the data set. A significant decrease in the GABAergic interneurons in DG-hilus in the injected side (*p = 0.0156, n = 7) compared to the non-injected side (Figure 3a). Also, a significant decrease in the number of GABAergic neurons was found in the injected side of CA1 (*p = 0.0156, n = 7) compared to the non-injected side (Figure 3b).

The analysis of total number of GABAergic interneurons in subject #13 in both DG-hilus and CA1 is provided in Figure 4. The datasets in these figures passed the Shapiro-Wilk normality test. There was a significant decrease in the GABAergic interneurons in DG-hilus in the injected side (*p = 0.0073, n = 3, paired t-test) compared to the non-injected side (Figure 4a). However, for CA1 SO and SR, there was not a significant decrease in the number of GABAergic neurons

found in the injected side of CA1 ($p = 0.1990$, $n = 3$, paired t-test) compared to the non-injected side (Figure 4b). The total number of GABAergic interneurons for CA3 SO and SR regions were not manually counted because they contained densely packed cells. The presence of GABAergic cells was marked by bright intensity cells. Therefore, the loss of GABAergic neurons was analyzed using integrated density which used the same region of interest (ROI) and determined the pixel intensity in the ROI while considering the area of the region.

An integrated density analysis of several brain regions of both injected and non-injected sides of subject #12 is seen in Figure 5. To test whether the injection of the viral vector was confined to the hippocampus an integrated density analysis was performed on the thalamus. There was not a significant difference ($p = 0.9663$, paired t-test) in the left or right sides of the thalamus (Figure 5a). This suggests that the injection did not result in a loss of GABAergic interneuron in the thalamus, as the pixel intensities were similar for both sides. CA1 SO and SR analysis showed that there was a significant decrease in integrated density ($*p = 0.0201$, $n = 7$, paired t-test) for the injected sides when compared to the non-injected sides (Figure 5b). The data set for CA3 SO and SR did not pass the Shapiro-Wilk test, so a Wilcoxon test was performed. There was a significant decrease in the integrated density of the injected side of CA3 SO and SR ($*p = 0.0156$, $n = 7$, paired t-test) when compared to the non-injected sides (Figure 5c). These results suggest that in both CA1 and CA3 regions, there was a decrease in the GABAergic neurons in the injected side compared to the non-injected side.

Integrated densities of several brain regions showing both injected and non-injected sides of subject 13 are presented in Figure 6. The results of the integrated density of the thalamus (Figure 6a) showed that there was no significant difference in the injected versus non-injected sides ($p = 0.1306$). Again, confirming the confinement of the viral vector administration to the

hippocampal areas. There was not a significant decrease in pixel intensity for the CA1 SO and SR injected sides ($p = 0.5484$, $n = 3$, paired t-test) when compared to the non-injected sides (Figure 6b). Although, this suggests there is not a decrease in GABAergic interneurons in the injected side of CA1 SO and SR, it is more likely that enough sections were not analyzed to establish significant change ($n = 3$). There is a significant decrease in the integrated density of the injected side of CA3 SO and SR ($*p = 0.0403$, $n = 3$) when compared to the non-injected sides (Figure 6c). This is similar to observed results in subject #12. Subjects #12 and #13 analysis for GABAergic interneuron counts and integrated analysis were not merged because they did not have the same number of analyzed sections.

Automated cell count results in DG and CA1 SO and SR were obtained from Cell Profiler software for subject #12 (Figure 7) because prior results relied on manual counting (Fig 3 and Fig 4). The total number of GABAergic neurons in the DG-hilus is presented in Figure 7a. The data set obtained from this region did not pass the Shapiro-Wilk normality test, therefore a Wilcoxon test was used for data analysis. There was a significant decrease in total number of GABAergic cells in the injected side when compared to the non-injected side ($*p = 0.0156$, $n =$ 7a). There was a significant decrease in the number of GABAergic cells in the injected side ($*p = 0.0036$, $n =7$) versus the non-injected side of the CA1 SO and SR region (Figure 7b). This shows that the decrease in GABAergic neuron cells count in the injected side from Figures 3 and 4 were not due to bias counting.

Automated cell count results in DG and CA1 SO and SR were also obtained from Cell Profiler software for subject #13 (Figure 8). There was a significant decrease in total number of GABAergic cells in the injected side of the DG ($*p = 0.0205$, $n = 3$) when compared to the non-injected side (Figure 8a). The data set obtained from CA1 in this region did not pass the Shapiro-

Wilk normality test, therefore a Wilcoxon test was used for data analysis. The analysis showed that there was a decrease in the number of GABAergic cells in the injected side (*p = 0.025, n =3) versus the non-injected side of the CA1 SO and SR region (Figure 8b). This shows that the AAV2 CAS injection did selectively ablate GABAergic neurons in the DG and CA1 SO and SR regions of the hippocampus.

Analyzing Association between ImageJ and Cell Profiler Results

A Pearson Correlation coefficient analysis was performed to test the closeness of agreement between the measured values of two methods: Image J and Cell profiler (Figure 9). The non-injected side of the DG (r = 0.96) from both methods of analysis perfectly correlate together, while the injected side of the DG from both methods also perfectly correlate (r = 1) together (Figure 9a). Also, the non-injected side of the CA1 from both methods of analysis perfectly correlated together (r = 0.99), while the injected side of the CA1 (r = 1) from both methods also perfectly correlated together (Figure 9b). This shows that the results obtained from ImageJ by manual cell counting and automated cell counting Cell Profiler agree with each other.

Loss of Neurons in Day 35 vs 160 and Significant Decrease in Size of Dentate Gyrus Closer to the Injection Site

A repeated measures Anova was performed to test how the injected hemispheres change as regards to time (35 vs 160 days). More specifically we were testing whether a larger number of neurons would be lost over a longer period. While a mixed-effects analysis was performed to understand how loss of neurons was dependent on the distance away from bregma. We found that there was significant decrease in the number of neurons in the injected side of the hilus

across day 160 compared to day 35 (*p = 0.0383) (Figure 10a). We also found that there was significant decrease in the size of the DG closer to the site of injection (*p=0.0354). This decrease is observed in the images in Figure 10b, as the left image shows the DG at 2.2mm and the right showing DG at 2.5mm. This decrease in size included what appeared to be degeneration of the granule cell neurons (as seen in) most likely due to overexcitation of these neurons due to loss of inhibitory neurons. This suggests that neurons closer to the site of insult were more susceptible to apoptosis.

Reactive Gliosis as a Characteristic of AAV2-Flex-taCaspa3-2A-TEVp-induced TLE

Representative images of reactive gliosis observed in the injected side of the hippocampus are shown in figure 11. The entire hippocampal area with significant increase in GFAP in the left side (injected), when compared to the right (non-injected side) of the brain is observed (Figure 11a). Enlarged images of DG hilus in both injected and non-injected sides show extensive GFAP in the injected side of the brain (Figure 11b). GFAP is a neuronal marker for glial cells, therefore its increased presence in the injected sides of the brain suggests that there was extensive gliosis occurring after the death of GABAergic cells in that hemisphere.

Discussion

This study sets out to pathologically characterize the new method of establishing TLE in a mice model using the AAV2-Flex-taCaspa3-2A-TEVp vector. It aimed to test if there was a decrease in total neurons in the DG, CA1 and CA3. We also aimed to show that this technique would result in a decrease in GABAergic neurons in the injected side with the neurons closer to the injection experiencing the most loss. Furthermore, we expected to see unilateral gliosis where the viral vector was injected.

The stereology analysis showed that there was a total decrease of neurons in the injected side of DG, CA1 and CA3 regions when compared to the non-injected side qualitatively and quantitatively. This shows that the viral vector was successful in eliminating neurons in the hippocampus proper. There was also an obvious shrinkage in the hippocampal circuit on the injected side compared to the non-injected side. The shrinkage seen in the injected side of the hippocampus mimics 50% to 75% of patients with epilepsy who develop hippocampal sclerosis Dendritic atrophy which eventually leads to shrinkage of cells and causes volume loss of the tissue (Anand and Dhikav, 2012).

Furthermore, images analyzed from subject Vgat-tom #12 and 13 specifically for GABAergic neuronal count showed that there was a decrease in the total GABAergic neurons in both DG, CA1 SO and SR. The pathological characterization of this study establishes that the protocol used is sufficient to selectively ablate GABAergic neurons permanently in the hippocampal regions. The loss of GABAergic interneurons in the injected side was enough to cause epilepsy in mice since each mouse experienced two or more SRSs because in humans, epilepsy is clinically defined as two or more unprovoked seizures occurring >24h apart (Fisher et al., 2014). Furthermore, the GABAergic interneuron ablation could be a form of traumatic brain injury (Brizuela et al., 2017, Blaiss et al., 2011) which is one of the causes of TLE, thus establishing a constructive validity for the model. Also, a loss of GABAergic neurons is typically seen in human TLE adding to the face validity of the model (Houser, 2015**)**. Also, because two methods: ImageJ and CellProfiler, were performed to analyze the total number of neurons, we ensured and found that the measured value from the two data sets agreed with one another.

Furthermore, we learned that there was a significant loss of neurons closer to the site of injection. This is similar to what is observed with human TLE as dying neurons causes axonal sprouting and synaptic-circuit reorganization proximal to site of injury thus contributing to epileptogenesis (Dingledine et al., 2015). Lastly, gliosis was observed in the injected sides of the brain when compared to the non-injected side. This is seen by the increased immunoreactivity of GFAP in the injected sides of both the hilus, CA1 and CA3. Gliosis is frequent in the human epileptic brain and seizures have been shown to frequently initiate within or very near gliotic brain tissues (Loewen et al., 2016). The results suggest that GABAergic cells in the hippocampus were mainly replaced by gliosis in the dentate gyrus, CA1 and CA3, where a high proportion of glial cells typically showed upregulation (Briellmann et al., 2002). This activity reflects changes important in the development of hippocampal epileptogenicity as human TLE tissue is also characterized by reactive gliosis, and glial scarring in the hippocampus (Loewen et al., 2016). Several studies suggest that glial cells have the ability to absorb the excess glutamate that is excreted during the increased activity of the glutamatergic nerve cells during normal brain functioning (Verdugo et al., 2019). Therefore, when an imbalance of excitation to inhibition is created by ablating GABAergic cells, there is a mechanism in place to increase gliosis in an effort to reduce glutamatergic transmission.

Future studies to understand the influence of GABAergic inhibition on seizure susceptibility as well as the interplay on genetics could be performed. Also, we could investigate the correlation between GABAergic neurons loss and seizure frequency (Buckmaster et al., 2017). This would help elucidate which abnormalities are epileptogenic, because if a pathological abnormality is epileptogenic, then its severity might correlate with the frequency of spontaneous seizures. Therapeutic options like replacing or protecting GABAergic interneurons

e.g., adenosine protection of GABAergic interneurons (Alfinito et al., 2003, Masino et al., 2018 and Löscher et al., 2010) could be performed to observed if this would prevent or reverse hippocampal damages and stop SRSs in mice.

In conclusion, this study was able to show that injecting the AAV2-Flex-taCaspa3-2A-TEVp viral vector unilaterally was able to create distinct TLE characteristics in the hippocampus. A decrease in neuronal cell counts as well as GABAergic interneurons was observed in DG, CA1 and CA3. Significant loss of neurons closer to the injection site was observed as well as a loss of hippocampal volume. Lastly, reactive gliosis is present in the injected side of the hippocampus.

Tables and Figures

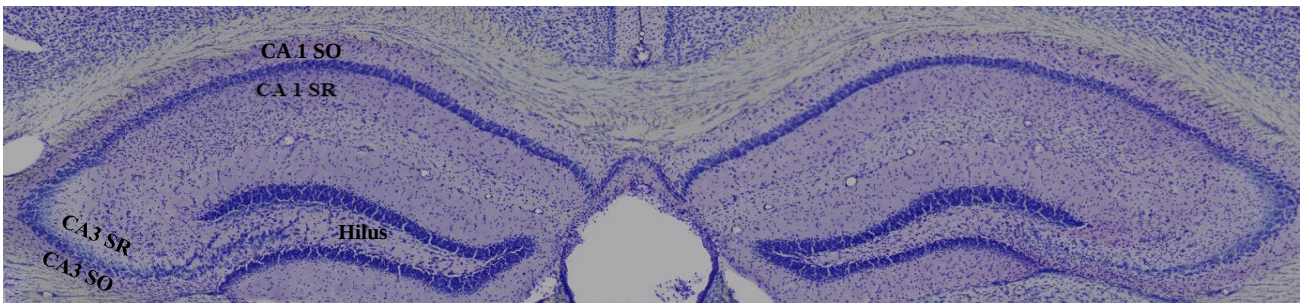

Figure 1. Nissl-stained section showing both non-injected and injected sides of the entire hippocampal circuit. (a) Representative image of Nissl section of both sides, non-injected (left), injected (right), showing the delineation of DG-Hilus, CA1 SO, CA1 SR, CA3 SO and CA3 SR.

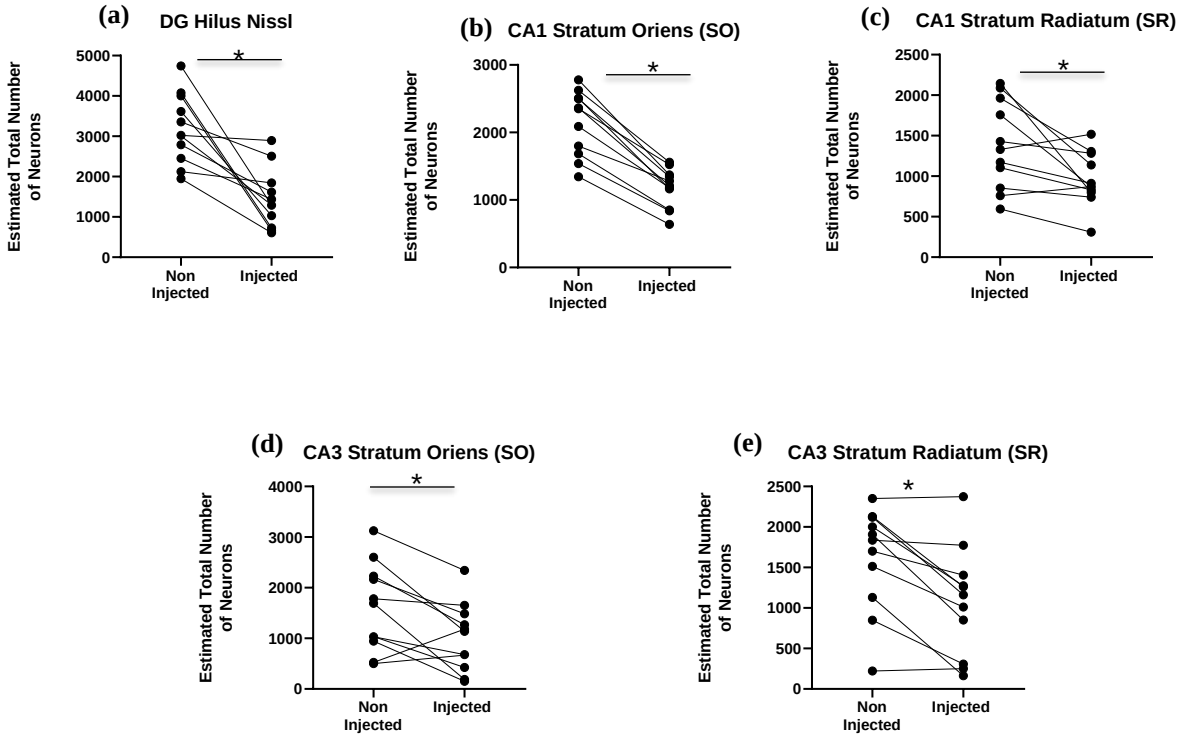

(f) Non-Injected Injected

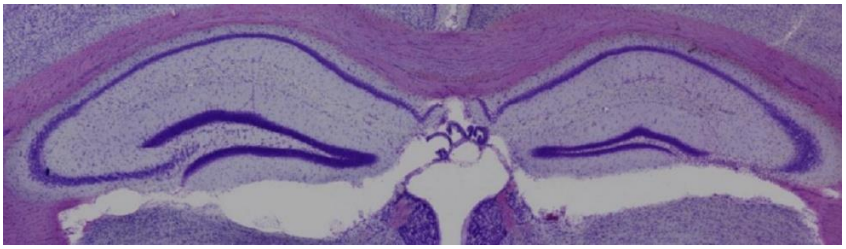

(g)

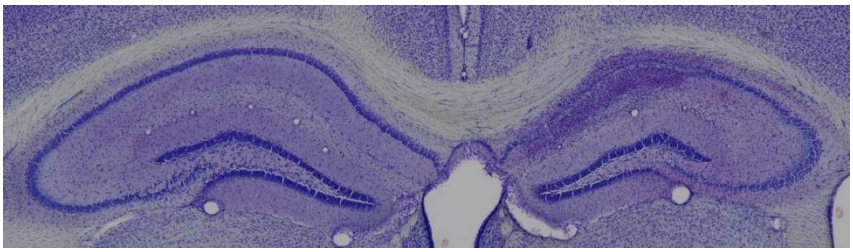

Figure 2. (a) Estimated total number of neuron count in each hippocampal region for both injected and nom-injected sides for all animals (n=11). All results shown are statistically significant as indicated by *. **(b)** Representative images showing decrease in injected hippocampal circuit and appearance of glia cells.

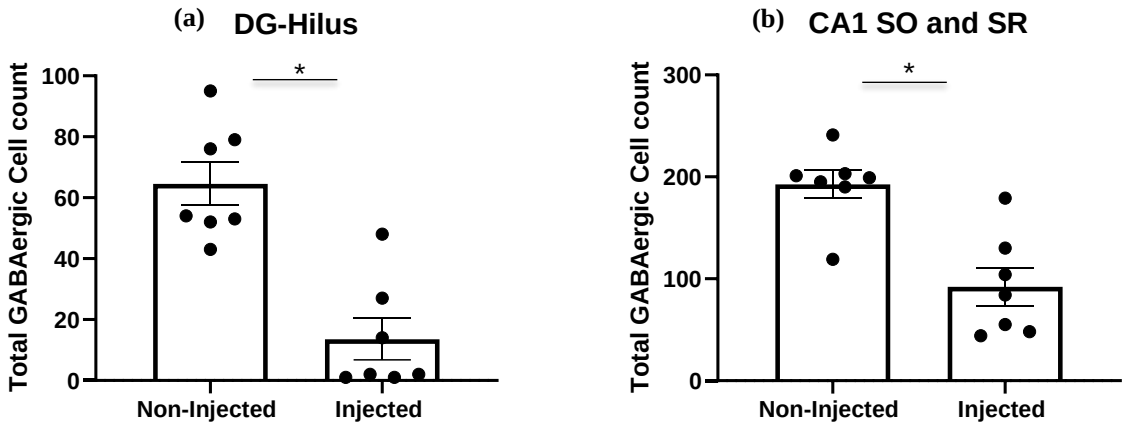

Figure 3. Total number of GABAergic cells counted in both injected and non-injected sides of the DG and CA1 for subject #12 section from ImageJ analysis.

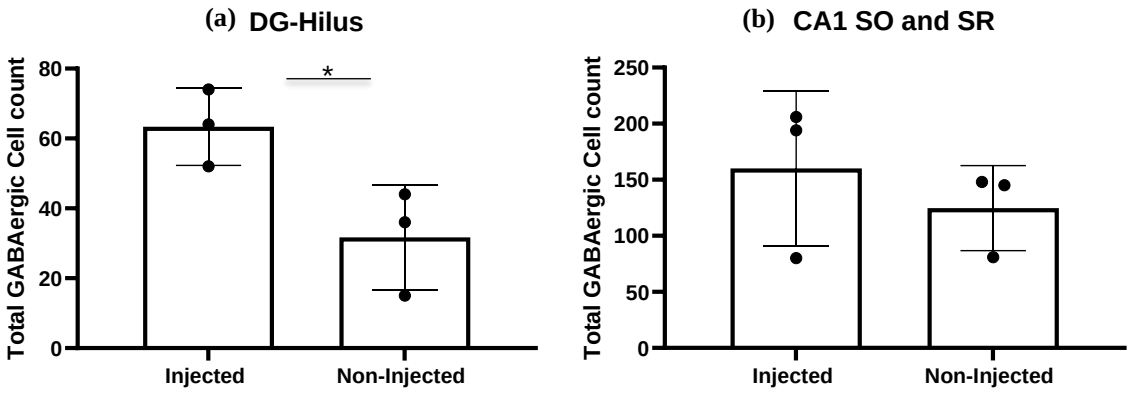

Figure 4. Total number of GABAergic cells counted in both injected and non-injected sides of the DG and CA1 for subject #13 sections from ImageJ analysis.

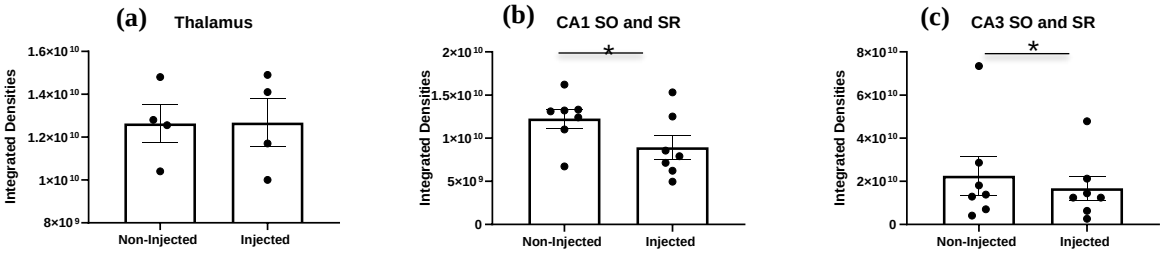

Figure 5. Integrated densities of thalamus, CA1 and CA3 showing both injected and non-injected sides of subject 12 sections from ImageJ analysis.

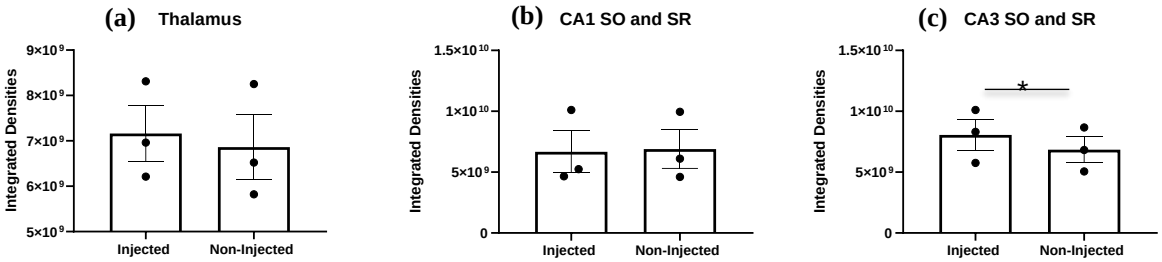

(d)

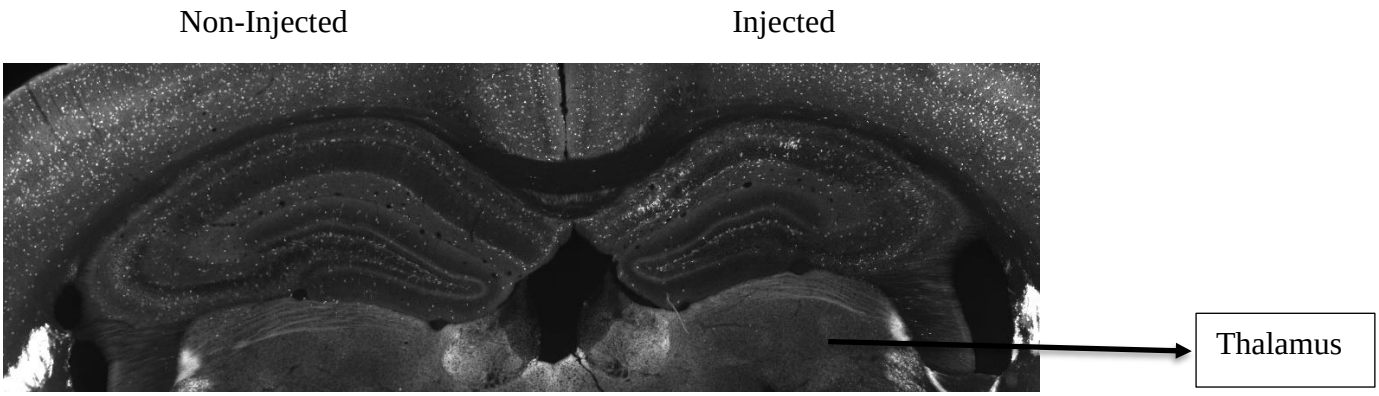

Figure 6. Integrated densities of CA1, CA3 and thalamus showing both injected and non-injected sides of subject 13 from ImageJ analysis.

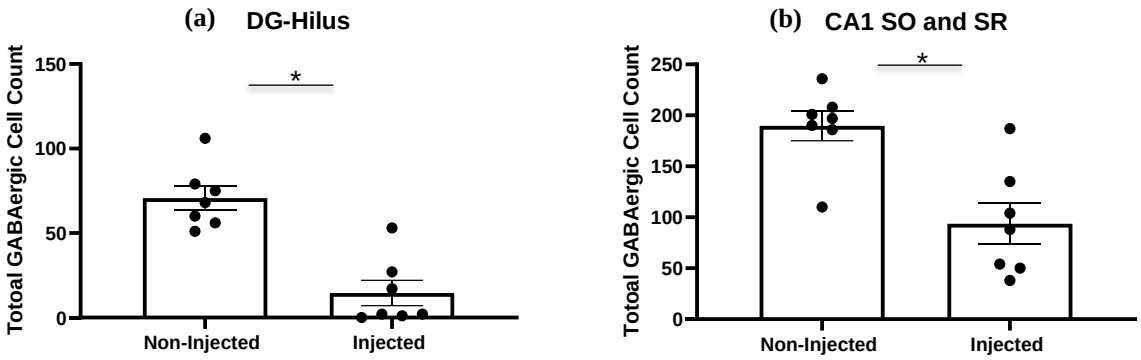

Figure 7. Total number of GABAergic cells counted in both injected and non-injected sides of the DG and CA1 for subject #12 sections.

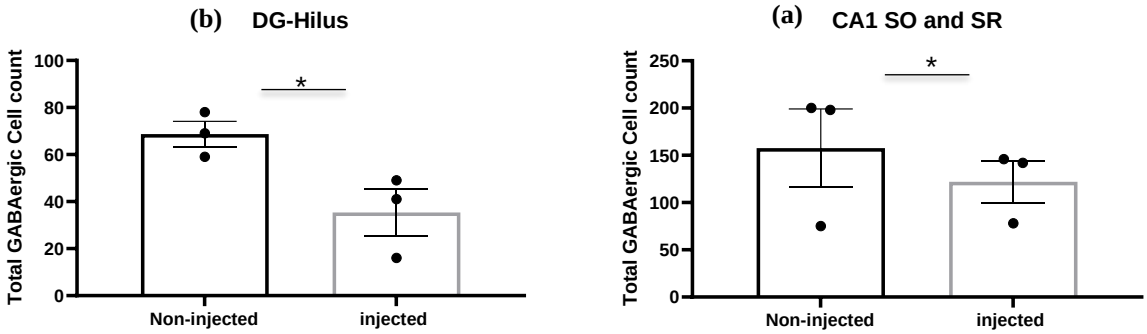

Figure 8. Total number of GABAergic cells counted in both injected and non-injected sides of the DG and CA1 for subject #13 sections.

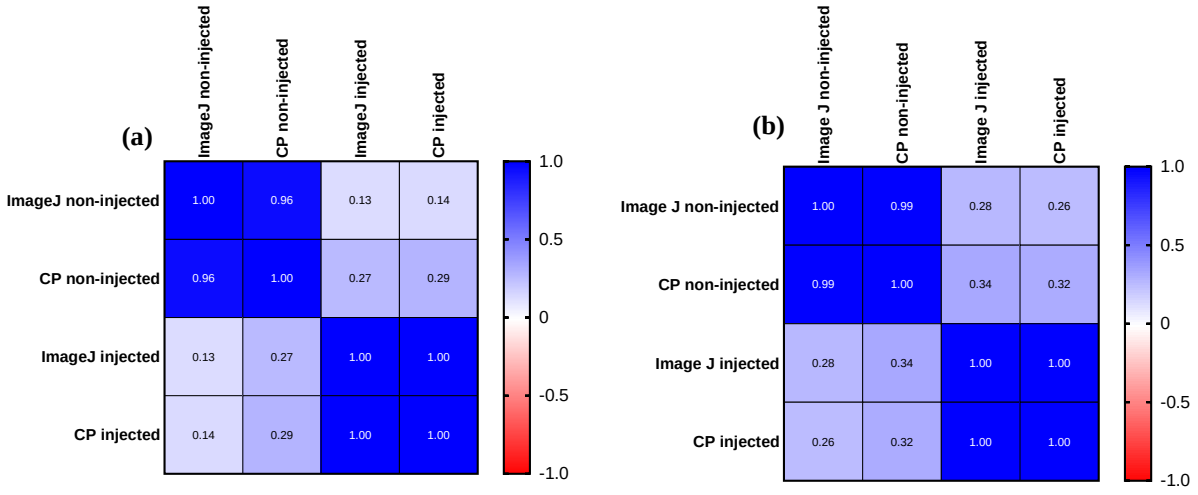

Figure 9. Pearson Correlation coefficient showing the closeness of agreement between the measured values of two methods: Image J and Cell Profiler. (9a) Shows the closes in the measure values of the injected and non-injected side of DG using ImageJ and Cell Profiler (CP) (9b) Shows the closes in the measure values of the injected and non-injected side of CA1 using ImageJ and Cell Profiler (CP)

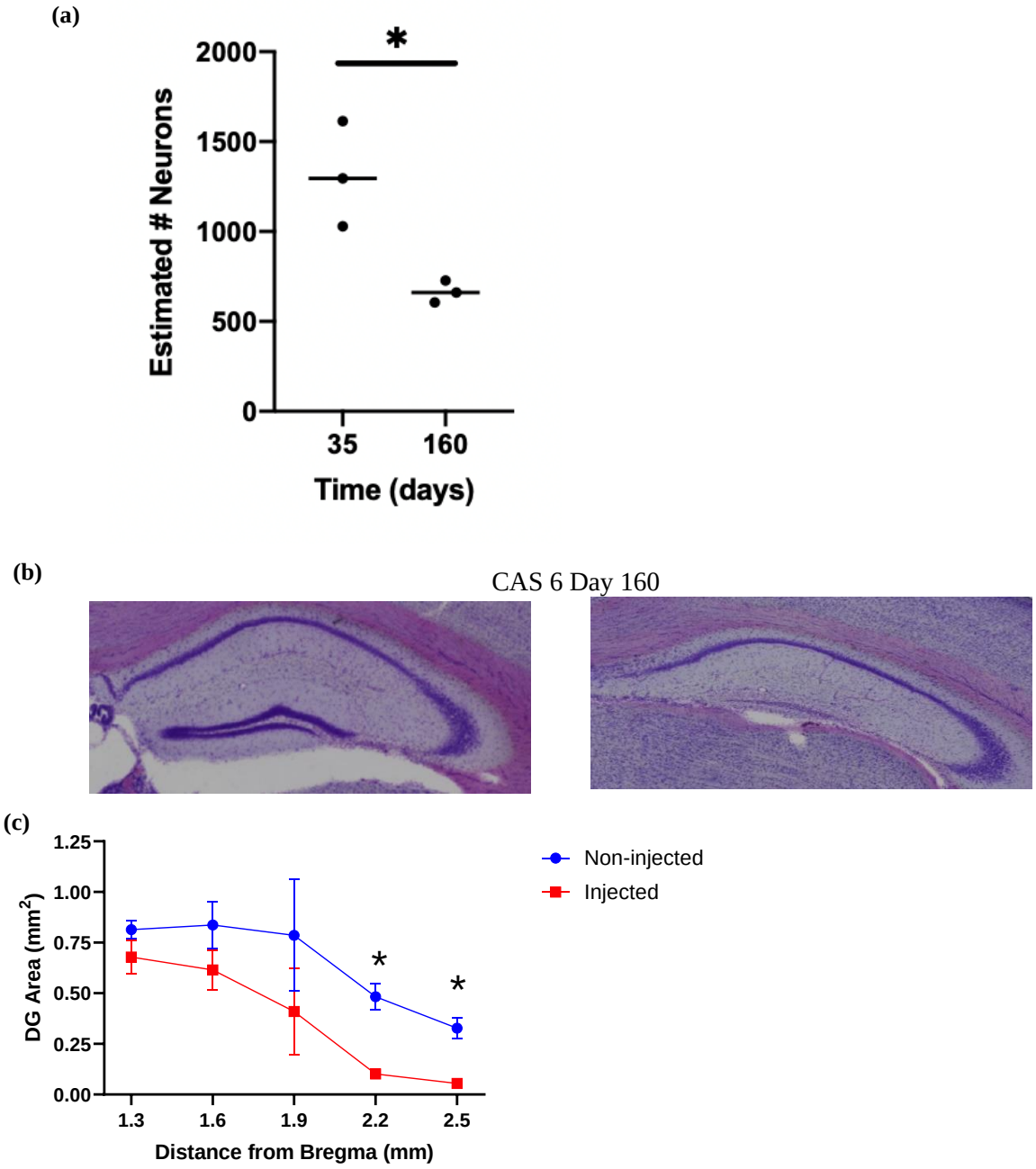

Figure 10. (a) Estimated number of neurons in the DG-Hilus showing an effect of side but not effect of time (days). **(b)** Representative images of injected side of CAS 6 after 160 days. Image on the left shows DG at 2.2mm, and image on the right shows DG at 2.5mm. **(c)** DG-hilus area along AP axis showing effect of distance from Bregma.

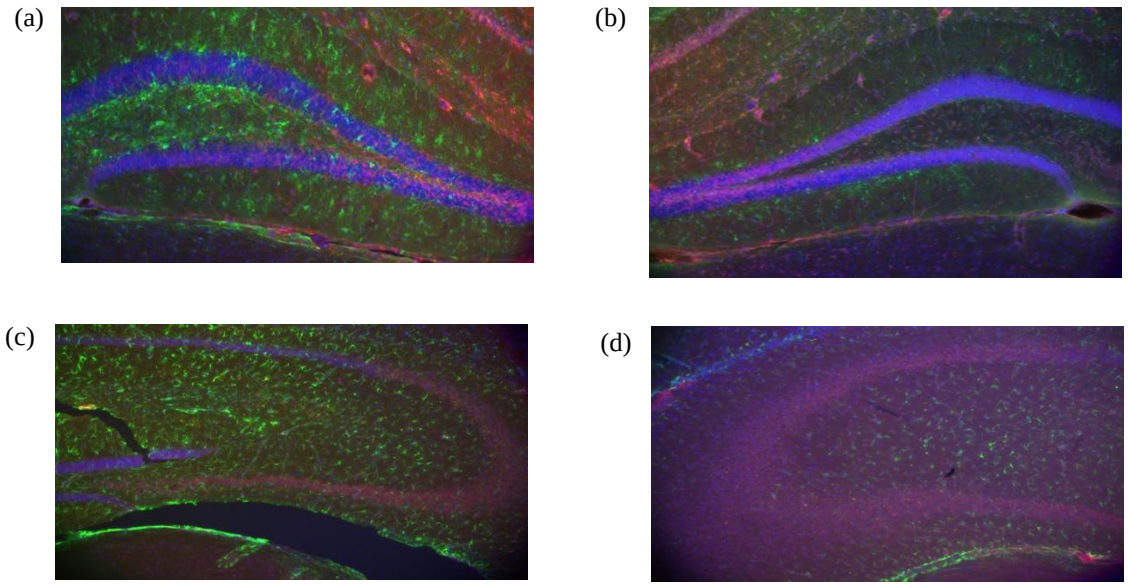

Figure 11. Representative images showing the reactive gliosis (indicated by appearance green color of GFAP) developed in the injected sides (left) of the dentate gyrus and CA3.

References

Ahmed Juvale, I. I., & Che Has, A. T. (2020). The evolution of the pilocarpine animal model of status epilepticus. *Heliyon*, *6*(7). https://doi.org/10.1016/j.heliyon.2020.e04557

Alfinito, P. D., Wang, S.-P., Manzino, L., Rijhsinghani, S., Zeevalk, G. D., & Sonsalla, P. K. (2003). Adenosinergic Protection of Dopaminergic and GABAergic Neurons against Mitochondrial Inhibition through Receptors Located in the Substantia Nigra and Striatum, Respectively. *The Journal of Neuroscience*, *23*(34), 10982–10987. https://doi.org/10.1523/JNEUROSCI.23-34-10982.2003

Anand, K. S., & Dhikav, V. (2012). Hippocampus in health and disease: An overview. *Annals of Indian Academy of Neurology*, *15*(4), 239–246. https://doi.org/10.4103/0972-2327.104323

Berger, M. L., Vass, K., Lassmann, H., & Hornykiewicz, O. (1990). The kainic acid model of human temporal lobe epilepsy: The superiority of intra-amygdaloid injection versus other application routes. In G. Lubec & G. A. Rosenthal (Eds.), *Amino Acids: Chemistry, Biology and Medicine* (pp. 455–464). Springer Netherlands. https://doi.org/10.1007/978-94-011-2262-7_54

Bird, C. W., Taylor, D. H., Pinkowski, N. J., Chavez, G. J., & Valenzuela, C. F. (2018). Long-term Reductions in the Population of GABAergic Interneurons in the Mouse Hippocampus following Developmental Ethanol Exposure. *Neuroscience*, *383*, 60–73. https://doi.org/10.1016/j.neuroscience.2018.05.003

Blaiss, C. A., Yu, T.-S., Zhang, G., Chen, J., Dimchev, G., Parada, L. F., Powell, C. M., & Kernie, S. G. (2011). Temporally Specified Genetic Ablation of Neurogenesis Impairs Cognitive Recovery after Traumatic Brain Injury. *The Journal of Neuroscience*, *31*(13), 4906–4916. https://doi.org/10.1523/JNEUROSCI.5265-10.2011

Briellmann, R. S., Kalnins, R. M., Berkovic, S. F., & Jackson, G. D. (2002). Hippocampal pathology in refractory temporal lobe epilepsy: T2-weighted signal change reflects dentate gliosis. *Neurology*, *58*(2), 265–271. https://doi.org/10.1212/wnl.58.2.265

Brizuela, M., Blizzard, C. A., Chuckowree, J. A., Pitman, K. A., Young, K. M., & Dickson, T. (2017). Mild Traumatic Brain Injury Leads to Decreased Inhibition and a Differential Response of Calretinin Positive Interneurons in the Injured Cortex. *Journal of Neurotrauma*, *34*(17), 2504–2517. https://doi.org/10.1089/neu.2017.4977

Buckmaster, P. S., Abrams, E., & Wen, X. (2017). Seizure frequency correlates with loss of dentate gyrus GABAergic neurons in a mouse model of temporal lobe epilepsy. *The Journal of Comparative Neurology*, *525*(11), 2592–2610. https://doi.org/10.1002/cne.24226

CellProfiler 3.0: Next-generation image processing for biology.

Chin, J., & Scharfman, H. E. (2013). Shared cognitive and behavioral impairments in epilepsy and Alzheimer's disease and potential underlying mechanisms. *Epilepsy & Behavior : E&B*, *26*(3), 343–351. https://doi.org/10.1016/j.yebeh.2012.11.040

Chun, E., Bumanglag, A. V., Burke, S. N., & Sloviter, R. S. (2019). Targeted hippocampal GABA neuron ablation by Stable Substance P–saporin causes hippocampal sclerosis and chronic epilepsy in rats. *Epilepsia*, *60*(5), e52–e57. https://doi.org/10.1111/epi.14723

Costa, M. S., Rocha, J. B. T., Perosa, S. R., Cavalheiro, E. A., & Naffah-Mazzacoratti, M. da G. (2004). Pilocarpine-induced status epilepticus increases glutamate release in rat hippocampal synaptosomes. *Neuroscience Letters*, *356*(1), 41–44. https://doi.org/10.1016/j.neulet.2003.11.019

Curia, G., Longo, D., Biagini, G., Jones, R. S. G., & Avoli, M. (2008). The pilocarpine model of temporal lobe epilepsy. *Journal of Neuroscience Methods*, *172*(2–4), 143–157. https://doi.org/10.1016/j.jneumeth.2008.04.019

Diaz Verdugo, C., Myren-Svelstad, S., Aydin, E., Van Hoeymissen, E., Deneubourg, C., Vanderhaeghe, S., Vancraeynest, J., Pelgrims, R., Cosacak, M. I., Muto, A., Kizil, C., Kawakami, K., Jurisch-Yaksi, N., & Yaksi, E. (2019). Glia-neuron interactions underlie state transitions to generalized seizures. *Nature Communications*, *10*(1), 3830. https://doi.org/10.1038/s41467-019-11739-z

Dingledine, R., Varvel, N. H., & Dudek, F. E. (2014). When and How Do Seizures Kill Neurons, and Is Cell Death Relevant to Epileptogenesis? *Advances in Experimental Medicine and Biology*, *813*, 109–122. https://doi.org/10.1007/978-94-017-8914-1_9

Drexel, M., Romanov, R. A., Wood, J., Weger, S., Heilbronn, R., Wulff, P., Tasan, R. O., Harkany, T., & Sperk, G. (2017). Selective Silencing of Hippocampal Parvalbumin Interneurons Induces Development of Recurrent Spontaneous Limbic Seizures in Mice. *Journal of Neuroscience*, *37*(34), 8166–8179. https://doi.org/10.1523/JNEUROSCI.3456-16.2017

Dudek, F. E. (2020). Loss of GABAergic Interneurons in Seizure-Induced Epileptogenesis—Two Decades Later and in a More Complex World. *Epilepsy Currents*, *20*(6 Suppl), 70S-72S. https://doi.org/10.1177/1535759720960464

Falcón-Moya, R., Losada-Ruiz, P., Sihra, T. S., & Rodríguez-Moreno, A. (2018). Cerebellar Kainate Receptor-Mediated Facilitation of Glutamate Release Requires Ca2+-Calmodulin and PKA. *Frontiers in Molecular Neuroscience*, *11*. https://doi.org/10.3389/fnmol.2018.00195

Fisher, R. S., Acevedo, C., Arzimanoglou, A., Bogacz, A., Cross, J. H., Elger, C. E., Engel, J., Forsgren, L., French, J. A., Glynn, M., Hesdorffer, D. C., Lee, B. I., Mathern, G. W., Moshé, S. L., Perucca, E., Scheffer, I. E., Tomson, T., Watanabe, M., & Wiebe, S. (2014). ILAE official report: A practical clinical definition of epilepsy. *Epilepsia*, *55*(4), 475–482. https://doi.org/10.1111/epi.12550

Fritsch, B., Qashu, F., Figueiredo, T. H., Aroniadou-Anderjaska, V., Rogawski, M. A., & Braga, M. F. M. (2009). Pathological alterations in GABAergic interneurons and reduced tonic inhibition in the basolateral amygdala during epileptogenesis. *Neuroscience*, *163*(1), 415–429. https://doi.org/10.1016/j.neuroscience.2009.06.034

Furtado, M. A., Castro, O. W., Del Vecchio, F., de Oliveira, J. A. C., & Garcia-Cairasco, N. (2011). Study of spontaneous recurrent seizures and morphological alterations after status epilepticus induced by intrahippocampal injection of pilocarpine. *Epilepsy & Behavior: E&B*, *20*(2), 257–266. https://doi.org/10.1016/j.yebeh.2010.11.024

Houser, C. R. (2014). Do Structural Changes in GABA Neurons Give Rise to the Epileptic State? *Advances in Experimental Medicine and Biology*, *813*, 151–160. https://doi.org/10.1007/978-94-017-8914-1_12

Hubbard, J. A., & Binder, D. K. (2016). Chapter 4—Types of Epilepsy. In J. A. Hubbard & D. K. Binder (Eds.), *Astrocytes and Epilepsy* (pp. 75–92). Academic Press. https://doi.org/10.1016/B978-0-12-802401-0.00004-1

Jensen, F. E., & Baram, T. Z. (2000). Developmental Seizures Induced by Common Early-Life Insults: Short- and Long-Term Effects on Seizure Susceptibility. *Mental Retardation and Developmental Disabilities Research Reviews*, *6*(4), 253–257. https://doi.org/10.1002/1098-2779(2000)6:4<253::AID-MRDD4>3.0.CO;2-P

Kandratavicius, L., Balista, P. A., Lopes-Aguiar, C., Ruggiero, R. N., Umeoka, E. H., Garcia-Cairasco, N., Bueno-Junior, L. S., & Leite, J. P. (2014). Animal models of epilepsy: Use and limitations. *Neuropsychiatric Disease and Treatment*, *10*, 1693–1705. https://doi.org/10.2147/NDT.S50371

Kapur, J. (2018). Role of NMDA receptors in the pathophysiology and treatment of status epilepticus. *Epilepsia Open*, *3*(Suppl Suppl 2), 165–168. https://doi.org/10.1002/epi4.12270

Kienzler-Norwood, F., Costard, L., Sadangi, C., Müller, P., Neubert, V., Bauer, S., Rosenow, F., & Norwood, B. A. (2017). A novel animal model of acquired human temporal lobe epilepsy based on the simultaneous administration of kainic acid and lorazepam. *Epilepsia*, *58*(2), 222–230. https://doi.org/10.1111/epi.13579

Knopp, A., Kivi, A., Wozny, C., Heinemann, U., & Behr, J. (2005). Cellular and network properties of the subiculum in the pilocarpine model of temporal lobe epilepsy. *Journal of Comparative Neurology*, *483*(4), 476–488. https://doi.org/10.1002/cne.20460

Lévesque, M., & Avoli, M. (2013). The kainic acid model of temporal lobe epilepsy. *Neuroscience and Biobehavioral Reviews*, *37*(10 Pt 2), 2887–2899. https://doi.org/10.1016/j.neubiorev.2013.10.011

Loewen, J. L., Barker-Haliski, M. L., Dahle, E. J., White, H. S., & Wilcox, K. S. (2016). Neuronal Injury, Gliosis, and Glial Proliferation in Two Models of Temporal Lobe Epilepsy. *Journal of Neuropathology and Experimental Neurology*, *75*(4), 366–378. https://doi.org/10.1093/jnen/nlw008

Löscher, W., & Brandt, C. (2010). Prevention or Modification of Epileptogenesis after Brain Insults: Experimental Approaches and Translational Research. *Pharmacological Reviews*, *62*(4), 668–700. https://doi.org/10.1124/pr.110.003046

Losonczy, A., Zhang, L., Shigemoto, R., Somogyi, P., & Nusser, Z. (2002). Cell type dependence and variability in the short-term plasticity of EPSCs in identified mouse hippocampal interneurones. *The Journal of Physiology*, *542*(Pt 1), 193–210. https://doi.org/10.1113/jphysiol.2002.020024

Maccaferri, G. (2005). Stratum oriens horizontal interneurone diversity and hippocampal network dynamics. *The Journal of Physiology*, *562*(Pt 1), 73–80. https://doi.org/10.1113/jphysiol.2004.077081

Masino, S. A., Kawamura, M., & Ruskin, D. N. (2014). Adenosine Receptors and Epilepsy: Current Evidence and Future Potential. *International Review of Neurobiology*, *119*, 233–255. https://doi.org/10.1016/B978-0-12-801022-8.00011-8

McKhann, G. M., Schoenfeld-McNeill, J., Born, D. E., Haglund, M. M., & Ojemann, G. A. (2000). Intraoperative hippocampal electrocorticography to predict the extent of hippocampal resection in temporal lobe epilepsy surgery. *Journal of Neurosurgery*, *93*(1), 44–52. https://doi.org/10.3171/jns.2000.93.1.0044

Ngugi, A. K., Bottomley, C., Kleinschmidt, I., Sander, J. W., & Newton, C. R. (2010). Estimation of the burden of active and life-time epilepsy: A meta-analytic approach. *Epilepsia*, *51*(5), 883–890. https://doi.org/10.1111/j.1528-1167.2009.02481.x

Rocha, L. (2009). PEPTIDES | Participation of Opioid Peptides in Epilepsy. In P. A. Schwartzkroin (Ed.), *Encyclopedia of Basic Epilepsy Research* (pp. 1104–1111). Academic Press. https://doi.org/10.1016/B978-012373961-2.00164-8

Rusina, E., Bernard, C., & Williamson, A. (2021). The Kainic acid models of Temporal Lobe Epilepsy. *Eneuro*, ENEURO.0337-20.2021. https://doi.org/10.1523/ENEURO.0337-20.2021

Stafstrom, C. E. (2005). The Role of the Subiculum in Epilepsy and Epileptogenesis. *Epilepsy Currents*, *5*(4), 121–129. https://doi.org/10.1111/j.1535-7511.2005.00049.x

Zack, M. M. (2017). National and State Estimates of the Numbers of Adults and Children with Active Epilepsy—United States, 2015. *MMWR. Morbidity and Mortality Weekly Report*, *66*. https://doi.org/10.15585/mmwr.mm6631a1

Zhao, F., Kang, H., You, Li., Rastogi, P., Venkatesh, D., & Chandra, M. (2014). Neuropsychological deficits in temporal lobe epilepsy: A comprehensive review. *Annals of Indian Academy of Neurology*, *17*(4), 374–382. https://doi.org/10.4103/0972-2327.144003

Zheng, X.-Y., Zhang, H.-L., Luo, Q., & Zhu, J. (2011). Kainic Acid-Induced Neurodegenerative Model: Potentials and Limitations. *Journal of Biomedicine and Biotechnology*, *2011*. https://doi.org/10.1155/2011/457079